FIRE AND HIGH TEMPERATURE BEHAVIOUR OF THERMAL MORTARS

Maria João Sobral Cordeiro Pupo Correia
Instituto Superior Técnico, Universidade de Lisboa, Lisboa, Portugal. mariajoaopc@tecnico.ulisboa.pt

Abstract: The EU has committed to reach net-zero CO_2 emissions by 2050. The decarbonization pathways included the implementation of regulations and standards that have driven the use of new building envelope systems made of composite materials with insulating properties to fulfil energy performance requirements. However, to fulfil these requirements, multi-layered insulation systems made of inflammable materials have been applied to building facades and a significant number of fire accidents have been registered during the last decade. The use of aerogel-based mortars has begun to be explored due to its improved thermal insulation properties; however, and despite its potentialy great high temperature behaviour, experimental studies about the fire behaviour of these materials are still not available in the literature. In this context, the present work aims at characterizing the fire and post-fire behaviours of an innovative thermal mortar with aerogel incorporation, including the comparison with one conventional solution, a thermal mortar with expanded polystyrene granules (EPS), and using a lime-based mortar, as reference. To this end, an extensive experimental campaign was developed, including (i) mechanical characterization tests; (ii) thermophysical ones; (iii) microstructural analyses; (iv) fire reaction tests to evaluate the contribution of materials to fire development; and (v) fire exposure tests whose results were used to determine/ calibrate thermal conductivity and specific heat at elevated temperatures. Within these procedures it was possible to compare the fire and high temperature behaviour of thermal mortars as well as suggest complementary parameters (beyond the standards) to evaluate high temperature and fire performance of these construction materials. The results showed that both thermal mortars are thermally unstable due to the susceptibility of polymeric constituents when subjected to high temperatures. Despite the referred instability, the aerogel-based mortar exhibited higher residual properties, proving that its constituents (in particular, aerogel) are less degraded by exposure to high temperatures.

Keywords: Aerogel; EPS; Thermal mortars; Fire behaviour; High temperatures

1 Introduction

1.1 General framework

Until 20 to 25 years ago, the fire spread over and in facades played only a minor role during a fire event in buildings, as the outer walls comprised (mostly) non-combustible materials, such as brick masonry or concrete coated with non-combustible renders. However, with the adoption of new composites (with the use of significant combustible materials), fire spread in building facades has become an increasing issue in recent years.

The EU has committed to reach net-zero CO_2 emissions by 2050. The decarbonization pathways included the implementation of regulations and standards that have driven the use of new building envelope systems made of composite materials with insulating properties to fulfil energy performance requirements. These measurements may have a significant importance on reaching the EU target since energy demand for daily use in the UE represents nearly 55% of the global energy consumption in buildings [1]. Heating is one of the predominant items in consumption of raw materials, i.e. coal, oil, or natural gas.

The usage of new systems and coating technologies has launched a significant utilization of combustible materials which are used as thermal insulators due to their low thermal conductivity. However, the damage caused in case of fire can thus become considerable due to higher fire spread, being most of them are combustible. In fact, fires on building facades have never been so prevalent [2]. According to a recent survey[3], the frequency of this type of fires has increased 7 times in 30 years.

Despite the undoubtedly good thermal performance of External Thermal Insulation Systems, ETICS, which provide an improved thermal comfort and contribute to energy savings, their fire behaviour raises serious concerns when the insulation layer is made of combustible materials such as EPS and XPS. Alongside the immediate and visible reported damages when ETICS are subjected to fire, some hidden potential risks also exist. An independent study by the University of Central Lancashire [4] found significant amounts of toxins in soils and high concentrations of potentially carcinogenic residues in the burnt debris of the Grenfell tower. Also, a study in the UK [5] showed that following the Grenfell fire, high concentrations of benzene were discovered 140 m away from the tower in amounts 25 to 40 times higher than normal. Based on the above, it can be concluded that good thermal performance it is often not balanced with sustainability and fire safety; in this context, innovative thermal mortars should be developed to fulfill both thermal performance and fire safety requirements.

1.2 Aerogel and thermal insulation systems

Aerogel is a gel composed of a microporous solid in which the dispersed phase is a gas [6].

The structure of the aerogel is composed of small spherical agglomerates of silica (SiO_2 particles), generally with dimensions between 2 and 5 nm, which are linked together in a chain shape forming a porous spatial network in which the pores present an average dimension of 20 to 40 nm, varying between 1 and 100 nm. Thus, aerogels with different particle and pore sizes can be obtained, as well as different porosity values, which in general are around 75 to 98% [7–10].

Silica aerogels not only act as high-performance thermal insulators but also have an inorganic structure, therefore, they are non-combustible.

Previous studies on aerogels have showed that at 200°C the viscosity of aggregated nanoparticles decreases enough so that there is relative movement between them to achieve structural

relaxation. This translates into a shrinkage of the pores and a decrease in the volume of the material. As the temperature increases, the viscosity of the particles becomes sufficiently low so that there is an increased aggregation and densification of particles, which can alter the transparency and thermal conductivity of the material. Upon reaching the glass transition temperature (≈0-800°C) the extreme densification and particle aggregation drastically changes the nanostructure within hours [11].

Aerogel has a great potential to be incorporated in different construction materials (such as in thermal mortars), improving their thermal performance and, in the case of insulation layers, allowing for the use of lower thicknesses of material for the same thermal requirements. Its great performance under high temperatures is a pro.

Aerogel contributes to a low-density mass, an increase in thermal and acoustic insulation, and, potentially, to an improved fire resistance. Owing to the hydrophobic nature of aerogel, the aerogel-enhanced renders have the advantage of being water repellent, which avoids water absorption, while they are water vapour permeable and more breathable than conventional renders, which prevents surface wetness [12].

The incorporation of silica aerogels into coating materials has only been recently investigated, with the first publication on the subject appearing in 2012 [13]. Stahl et al. [13] presented a cementless mineral hydrophobic mortar with high thermal performance (0.025 W/(m.K)) and a density mass of 200 kg/m^3, with the incorporation of aerogel in 60 to 90% of the total volume, and some unidentified additions to improve workability. However, no mechanical performance, water behaviour or other fundamental properties, that allow a complete evaluation of the mortars, were referred.

As a matter of a fact, very few aerogel mortars can be found on the market. Among the first commercially available products, the "FIXIT222" was delivered with a declared thermal conductivity, λ, of 0.0261 W/(m.K) and a fire reaction class A2 [14], and several studies was conducted on this product [15, 16]. In fact, these materials are formulated with a complex mixture of several components. Apart from binders and aggregates, further additives provide specific and mandatory characteristics such as workability, adhesiveness and cohesion. The type and percentage of additives used (sometimes polymeric) can affect the final performance of the composite.

The main objective of this study was to compare a aerogel-based mortar with a conventional thermal mortar with EPS granules, using a traditional lime-based mortar as reference. The performance prior and after exposure to elevated temperatures and fire, as well as their post-fire (i.e. residual) behaviour, was evaluated. The goal was not only to characterize the thermophysical properties of the mortars at different elevated temperatures, but also to understand the degradation of the materials after exposure to high temperatures, namely in terms of residual mechanical resistance and changes in their microstructure.

2 Materials and experimental methods

2.1 Material characterization

The experimental campaign focused on the following 3 pre-dosed mortars: i) a conventional coating mortar based on natural hydraulic lime (Lime.m); and 2 thermal mortars, ii) one with EPS (EPS.m) aggregates and iii) the second one with silica aerogel granules (Aero.m). Table 1 summarizes the main properties of the materials; for Lime.m and EPS.m the values were provided by the manufacturer, while the ones from the Aero.m were collected from a PhD thesis whose focus consisted in analysing and studying the addition of fibbers to an aerogel-based mortar developed at PEP project *(P2020 POCI-01-0247-FEDER-017417)* [17]. The comparison is made, therefore, between two commercial mortars and a non-commercial one which was developed in the framework of the above-mentioned project.

The aerogel-based thermal render is composed of a blend of mineral binders (Portland cement and calcium aluminate cement), rheological agents, resins, hydrophobic agents, among others, while also containing, as lightweight aggregate and thermal insulation material, a commercial supercritical hydrophobic silica aerogel available in granules (particle size ≤ 3500 µm, apparent density ≤ 90 kg/m^3, particle compressive strength ≤ 0.80 MPa, and a thermal conductivity ≤ 0.020 W/(mK)) [18]. The mineral binders represented a total of 20 % (m/m), and silica aerogel hydrophobic granules a total of ≈ 37% (m/m), with the remaining quantities allocated to the other components [19].

Table 1. Properties of the mortars in study

ID	ρ kg/m^3	$\lambda_{10°C, dry}$ W/(m.K)	σ_T N/mm^2	σ_C N/mm^2	FR	Ref.
Lime.m	1500 - 1600	0.82	≤ 1.5	≤ 3.5	A1	[20]
EPS.m	150 ± 5	0.042	≥ 0.25	CSI (0.4 - 2.5)	B	[21]
Aero.m	160 ± 3	0.0293	0.099 ± 0.004	0.227 ± 0.002	-	[19]

ρ = dry bulk density; **$\lambda_{10°C, dry}$ =** thermal conductivity at 10°C and dry state; **σ_T =** flexural strength; **σ_C=**compression strength; **FR** = fire reaction class

2.2 Experimental methods

The work developed can be divided in two main categories: an experimental campaign (summarized in Figure 1) and a numerical analysis.

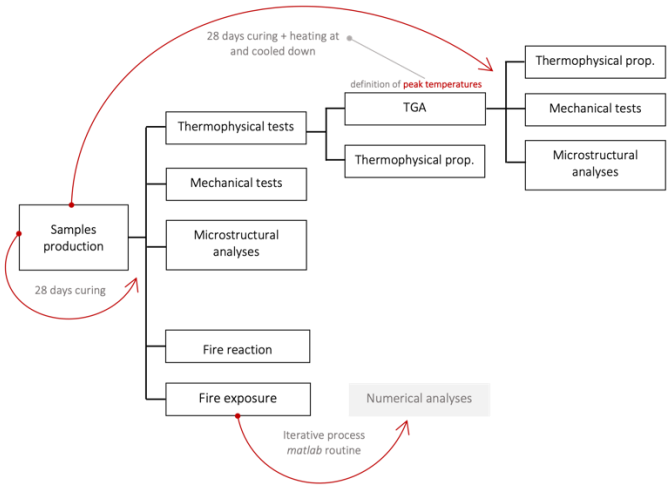

Figure 1. Flowchart explaining the experimental campaign

The experimental programme included the following main types of experiments: (i) material characterization tests to evaluate the flexural and compressive strengths, and thermophysical ones to measure thermal conductivity and specific heat; these tests were performed on reference specimens (i.e. without thermal damage) and on specimens after being subjected to a significant thermal damage

(exposure up to 400 °C), to understand how these properties were affected by temperature. Within thermophysical testing, thermogravimetric analysis (TGA) was also carried out, and according to the thermograms obtained, peak temperatures were found (temperatures in which the mass loss was most significant) and the temperature to measure thermal damage (≈400°C) was defined. (ii) Microstructural analyses: XRD, Micro CT, and SEM were useful to assess the performance and response of materials to heating. (iii) Fire reaction tests were also performed, giving values used by EU norms, therefore, essential to compare with commercial products and to understand how the materials contribute to fire development. Finally, (iv) fire exposure tests, in which specimens of the three thermal mortars were subjected to standard fire curve ISO-834 [22]. During the experiments, the temperature across the thickness was measured. These data were then used in an inverse numerical procedure in which thermal conductivity and specific heat at high temperatures were calibrated based on experimental thermal distributions.

The evaluated properties/ parameters are presented in Table 2.

Table 2. Synthesis of the tests and parameters measured

	Type of test			Parameter(s)
Specimens' production	(i) Characterization tests	Mechanical		σ_C
				σ_T
		Thermophysical	ISOMET 2114	λ
				Cp
			TGA	% of mass loss
	(ii) Microstructural Analyses	XRD		Id. mineral compounds
		Micro CT		High resolution images
		SEM		
	(iii) Fire Reaction tests	Ignitability		Flame spread, F_S
		Gross Calorific Potential		PCS
		Cone calorimeter		T_{ig}
		Bomb calorimeter		Heat release
	(iv) Fire exposure tests			Temperature along thickness while exposure to fire curve

σ_C = compression strength; σ_T = flexural strength; λ = thermal conductivity; Cp = specific heat; F_S = flame spread; T_{ig} = time to ignition

2.2.1 Mechanical tests

The mechanical performance of materials at the hardened state was evaluated to by means of compressive and flexural tests. Considering the requirements of the EN 998-1, the minimum value of compressive strength is associated to class CS I, which is 0.40 MPa, while for flexural strength no requirements are defined.

The maximum compressive and flexural stresses were measured with a *Form+Test* (*model 505/200/10/DM1*) equipment , with a load cell of 200kN for the compression test (testing speed of 5 mm/min) and 10kN for the flexural test (testing speed of 10 mm/min), using square prisms of 160x40x40 mm^3 and following the EN 1015-11 standard [23].

The specimens used for the flexural tests, after resulting in two halves, were used for carrying out the compressive tests.

These procedures were followed at i) room temperature, after 28 days of curing, for both flexural and compressive strength and ii) after the specimens had been heated up to 400°C to measure the residual compressive strength. The residual flexural strength was not measured since the magnitude of this value was expected to be extremely low.

The heating process was set up in a muffle furnace from room temperature until 410°C at rate of 10°C/min. To measure the temperature inside the material during heating, dummy specimens were instrumented with a thermocouple in their geometrical centre. The specimens were introduced inside the muffle until had passed 5 min since the interior of the material reached 400°C. Then, the equipment was turned off and the specimens were cooled down up to room temperature.

2.2.2 Thermophysical tests

i) Thermal conductivity and specific heat

The evaluation of the thermal conductivity and specific heat was carried out, after the 28-day curing period, through a transient method with the ISOMET 2114 equipment [24], which follows the ASTM D5930-9 standard test [25]. The equipment directly provides the value of thermal conductivity, λ, as well as the volumetric heat capacity, *cp*. The specific heat, *Cp*, is calculated by dividing the volumetric heat capacity by the bulk density, ρ. The bulk density was determined according to EN ISO 1015-10 [26].

To analyse the aerogel-based mortar, cylindrical specimens with 40 mm diameter and 100 mm of height were made, and it was used the needle probe exhibiting a measurement range between 0.015 and 0.050 W/(m.K), with an accuracy of 5 % of the reading value + 0.001 W/(m.K) and reproducibility of 3 % + 0.001 W/(m.K). For EPS.m and for Lime.m samples with 60 mm diameter and 20 mm of thickness were produced and it was used the surface probe exhibiting a measurement range between 0.04 and 6 W/(m.K) with an accuracy of 10 % of the reading value and reproducibility of 3 % + 0.001 W/(m.K) [24].

The procedure took place at i) room temperature, after 28 days of curing and ii) after the specimens had been heated up to 400°C to measure the residual thermal conductivity. The heating process was the same as the one described in section 2.2.1.

ii) TGA

The mortar samples were analyzed using a *Netzsch STA 409 PC* thermobalance, under air flow (oxidizing atmosphere), and at a heating rate of 25°C/min. The samples, 60-100 mg (fragments), were heated from room temperature to 1100°C using alumina crucibles. The heating rate was optimized to make the different thermal decomposition processes clear and with as lower overlap as possible. For each thermogram acquired the thermal decomposition rate (DTG), which is the derivate of the initial thermogram, was calculated using the Proteus software of the equipment.

2.2.3 Microstructural techniques

The samples were analysed by X-Ray diffraction (XRD) and Micro computed tomography (Micro CT), both at room temperature and after heating up the specimens in a muffle at 300°C in a muffle and cooled down. These procedures were used to analyse the changes on microstructure due to high temperature exposure. The microstructural tests were only carried out on thermal mortars, EPS.m and Aero.m.

This temperature was set to take advantage of the fact some preliminary specimens had been heated up to 300 °C (before the target value of 400 °C had been decided based on the TGA results).

i) X- Ray diffraction (XRD)

The X-ray diffraction (XRD) test allows the qualitative identification of the crystalline compounds in the sample and evaluates the presence of amorphous phases.
A diffractogram contains several peaks that are characterized by their position, intensity and shape. Each phase/substance has a characteristic X-ray diffractogram.
Phase identification is performed by comparing the diffractogram of an unknown sample with diffractograms from a reference database (PDF4 ®).
An X-ray diffractometer (*X'Pert PRO* from *Panalytical*) was used for this test, with a copper ampule (K-Alpha 1.541). The current intensity used was 35 mA, with a voltage of 40 kV. Scans were performed from 5° to 70° of 2θ, with a step of 0.033° and t=75 seconds per step.

i) Micro computed tomography (Micro CT)

Micro computed tomography is a 3D, high-resolution X-ray imaging. The obtained radiographs are strongly dependent on the composition and microstructure of the studied objects. The acquisition was made with the SKYSCAN 1144 (Brucker) scanner, with 59 kV Source Voltage and 167 µA Source Current. The Image Pixel Size is 5.07 µm, and the rotation step is 0.3°, using 5 frame averaging and a 180° scan.

ii) Scanning electron microscope (SEM)

Scanning electron microscopy (SEM) analysis was carried out using both a SEM Hitachi S-2400, working at an acceleration voltage of 20kV and coupled with an Oxford Inca X-Sight energy dispersive X-ray spectrometer, and a SEM Thermoscientific Phenom ProX G6, working at an acceleration voltage of 15 or 20 kV. Samples were previously sputtered with a Pt-Au coating.

2.2.4 Fire reaction tests

i) Ignitability test

The ignitability test can be considered as a small-scale reaction-to-fire test; its main objective is to determine the ignitability of a material by exposing a sample positioned vertically to a small flame inside a combustion chamber -a detailed description is provided in ISO 11925-2.
The evaluation of ignitability is established by measuring the flame propagation distance and total duration of the test. The ignition of the filter paper positioned under the sample due to falling drops and ignited particles is also observed.
The sample to be tested shall be 250 mm x 90 mm and a maximum thickness of 60 mm.
The duration of the test is 30s with 15s of flame imposition. During this time, it is intended to determine whether the distance of 150 mm is reached (the flame spread (F_S) in mm is measured), as well as to assess the combustion of the filter paper placed inside the chamber.

ii) Gross calorific potential test

To determine the calorific value according to EN ISO 1716, the sample is subjected to complete combustion in a constant volume containing oxygen under pressure with high purity. The occurrence of combustion is indicated by a temperature rise, which allows the determination of the calorific value. This quantity is intended to characterise the amount of heat released by the material per unit mass (PCS – gross calorific potential), in MJ/kg, when subjected to complete combustion.
A sample of material reduced to powder and of known mass is mixed with the same quantity of paraffin and introduced into the calorimetric pump where the test is carried out.

iii) Cone calorimeter

The cone calorimeter uses radiant heat to ignite the samples (Figure 2(left)). To avoid ignition of the edges of the specimen, the sample is enclosed in a steel frame (Figure 2(right)), that ensures ignition of the surface.
This equipment is used to calculate the time to ignition of a material. The specimens used are 10 cm x 10 cm in cross section and 3 cm in thickness.
The material sample is measured and weighed before it is placed in the steel frame; then the samples is placed 25mm below the cone and the test is ready to begin. The cover of the heating element is opened, and the piloted spark ignition is activated. From opening the cover, a timer is started to measure the point where the sample ignites.
The test is performed (Figure 2(right)) with different heat fluxes until the critical flux is found, i.e. the minimum heat flux to ignite the surface.
The specimens were made at LC in IST and the test took place at a Fire Lab in DTU.

Figure 2. Cone calorimeter test: equipment (left), ongoing test (right)

iv) Bomb calorimeter

Combustion calorimeters measure the heat released from a combustible material (solid or liquid). This is done by weighing a precise measure (a few milligrams) of the sample substance into a crucible which is placed inside the "bomb," a sealed metal cylinder called vessel, filling the vessel with oxygen (~ 30 bar), and igniting the substance. The sample burns and the resulting temperature increase of the vessel is measured and from it the calorific value is calculates by comparing it to a previous combustion of a known substance, calibration.

2.2.5 Fire exposure tests

The experimental campaign included fire exposure tests, in which the specimens are subjected to a heating curve according to the standard fire defined in ISO 834. The 3 mortars were applied with a thickness of 40 mm on 5 mm thick steel plate, where the thermal action took place. To perform the temperature measurements along the mortar thickness, type K

thermocouples (conductor diameter of 0.25 mm) were positioned with a vertical spacing of 10 mm during the samples' preparation.

The temperature measurements were acquired at a 1 Hz rate, using a datalogger (*HBM, model Quantum X MX1609*) connected to a computer. The test duration was defined according to the temperature up to which the properties were intended to be calibrated. The limit was set at 800 °C, as the degradation of thermal mortars was already significant due to the presence of polymeric compounds.

The tests took place in a furnace with exterior dimensions of 2.10 m (height) x 1.25 m (width) x 1.20 m (depth) and a top opening area of 0.60 m x 0.30 m (Figure 3). The steel plate had the exact same dimensions to cover the opening. As the mortar area was 0.20 m x 0.20 m, the remain part of the plate was covered with an insulation material – ceramic wool; this procedure guaranteed proper insulation of the lateral sides of the mortar which was especially relevant since it was pretended the heat flow to be unidirectional – ascending.

The minimization of convection phenomena in the air above the mortar was accomplished by covering the space between the exhaust system and the specimen with a non-flammable fabric.

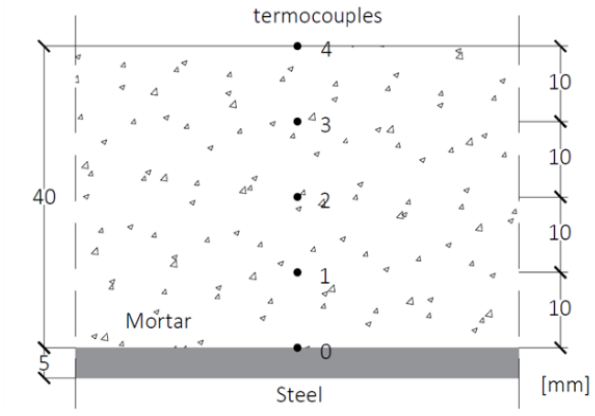

Figure 3. Test setup: general view (top); scheme of thermocouples disposal inside the mortar (bottom)

3 Results and discussion

3.1 Mechanical tests

Considering the mechanical properties at room temperature, thermal mortars have a significant less flexural and compressive strength than Lime.m (Figure 4). However, this is not a problem insofar as this type of mortars is to be used as part of a system that already foresees this vulnerability and, therefore, relies on a fiberglass mesh as reinforcement. As observed in Figure 4, Aero.m present the lowest initial mechanical properties; this can be related to the high percentage (≈37%) of aerogel granules in this mortar since aerogel is fragile and has a porous matrix.

When comparing the residual compressive strength with the values obtained at room temperature and looking at Figure 4, it can be seen that Lime.m presents a slight decrease of 4% resistance. By evaluating the thermal mortars, the pattern is completely different. The highest decrease in compressive strength is observed in EPS.m (91%) that reaches lower values than the ones obtained for Aero.m, which can be justified by the higher polymeric content of the former mortar.

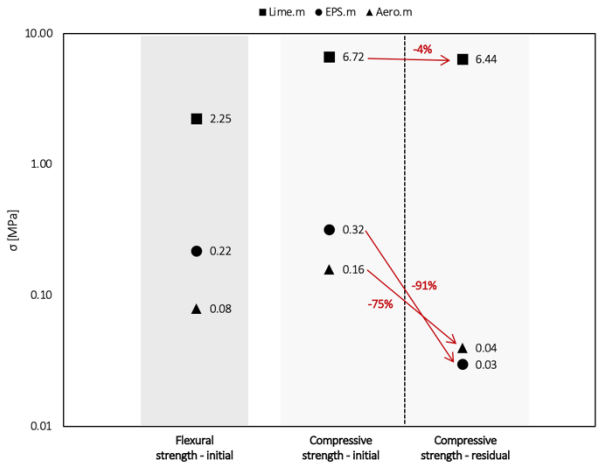

Figure 4. Average values of the initial and residual mechanical properties strength (after exposure to ≈ 400°C)

3.2 Thermophysical tests

i) Thermal conductivity and specific heat

When comparing the results obtained for the initial and residual specific heat and thermal conductivity shown in Figure 5, it is noticeable that the *Cp* of Aero.m is the most affected by temperature, whereas the one less affected is that of Lime.m. The higher susceptibility of the *Cp* of Aero.m can be justified by the degradation of (high) polymeric content (which is incorporated in these mortars to improve its initial mechanical properties). Since these components are no longer present after heating, the thermal properties changed; this result means that it is required less energy to raise the temperature in Aero.m, which means lower *Cp*.

Regarding effect of temperature on the thermal conductivity (Figure 5), it can be concluded that thermal mortars have almost no variation while Lime.m decreases its λ in about 28%. This significant reduction observed on Lime.m, may be due to the mass loss (water evaporation) and the consequent increase of empty spaces/ pores, causing an improvement (i.e. reduction) on λ; additionally it can also be related the degradation on some components that had a higher thermal conductivity than the air that fill the remnants voids.

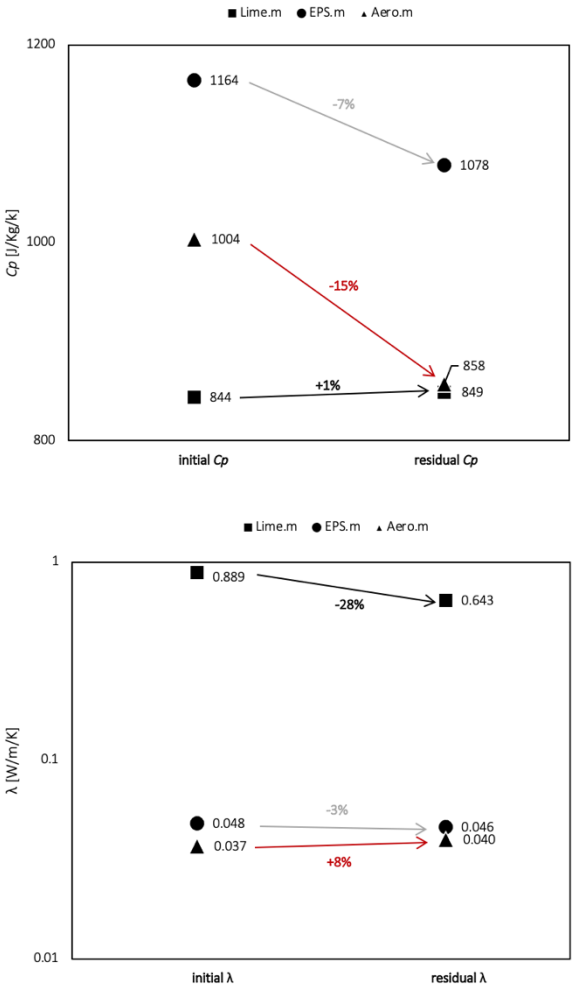

Figure 5. Initial and residual specific heat (top) and thermal conductivity (bottom)

ii) TGA

The thermograms of the thermal mortars with EPS and aerogel are distinct from the thermogram of the lime-base (reference) mortar, as can be clearly seen in Figure 6; the thermogram of the latter mortar exhibit an expected peak centered at around 850 °C, which corresponds to the decarbonation process of $CaCO_3$. The temperature range at which this process occurs depends on factors such as the size of the $CaCO_3$ particles and their degree of crystallinity [27]. This process also includes decarbonation of the calcium silicates in the mortar [28]. The mortar with aerogel has less calcite than the remaining two samples. Both thermal mortars exhibit a complex decomposition process between 250°C and 450°C, absent in the reference mortar. The decomposition process of the polymer component and polystyrene (at 350 °C) is visible for the EPS mortars. The thermal mortars also show decomposition processes at low temperature attributable to the dehydration of CSH, ettringite and stratlingite (225°C, only in the one with aerogel).

The three mortars analyzed present different residual masses at 1100 °C, due to their different percentages of calcite, portlandite and organic material from polystyrene and aerogel. It is worth mentioning the fact that the samples used in thermogravimetry have a small volume, therefore the results presented above may have a limited representativeness of a real application, in which relatively thick layers (i.e volume) of mortar are used.

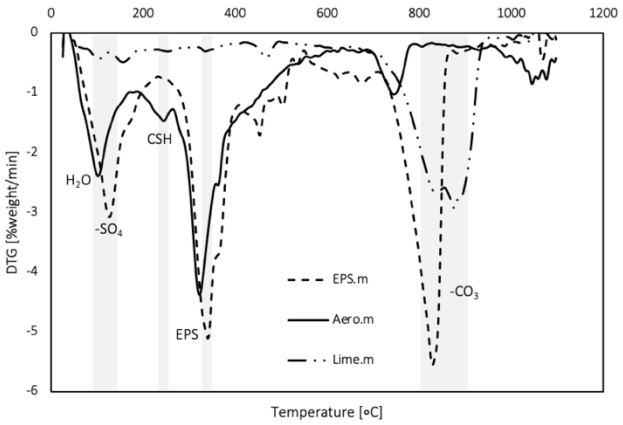

Figure 6. Thermogram DTG, of the prepared mortars (heating rate 25 °C/min, under air flow)

3.3 Microstructural analyses

i) X-Ray diffraction (XRD)

The X-ray diffraction pattern of Aero.m at initial conditions reveals the presence of calcite ($CaCO_3$), gypsum ($CaSO_4$), and gehlenite ($Ca_2Al_2SiO_7$). In the post heating pattern, it is noticeable the dehydration process since the representative peaks of gypsum and gehlenite disappear. In both graphs there is a slope between 15° and 35°, which are related to the presence of amorphous/nanocrystalline compounds.

Regarding the pattern of EPS.m at initial conditions, the only detected mineral was calcite, confirming the lime-based matrix of the mortar. However, as a sample from an old production was used in this test, most of the water had already evaporated, which led the complete carbonation of the material, which can explain the fact that only calcite was detected. The sample used for post heating analyses was recent, therefore it contains portlandite ($Ca(OH)_2$) that, when heated, generates intermediate (metastable) products. In fact, when heated, water is released and burnt lime (CaO) is reactivated again, promoting the formation of new carbonates, i.e. $CaCO_3$ polymorphs (vaterite and aragonite). The presence of these polymorphs can be attributed to fast carbonation after heating process.

Results showed that Aero.m had a cementitious matrix, whereas EPS.m presented a lime-based matrix.

ii) Micro CT

This nondestructive technique, enables the 3D visualization of objects, based in reconstructed images (slices). The radiation does not detect low dense or lightweight components such as the aggregates, EPS and aerogel, which comprise the thermal mortar analyzed, leading to apparent pores/ voids in the images.

The results presented do not show significant differences between the initial specimens and the post-heated ones. This technique allows the analyses of the matrix, and it can be concluded that there is no collapse or micro fissures due to the exposure to high temperature, which means the porous network was preserved.

To add value to these analyses, high-resolution pictures were taken, as shown in Figure 7. The EPS has a honeycomb structure after heating, with a probably more rigid (and presumable brittle) structure resulting from the decomposition of the polymeric components (justifying in part the loss of mechanical strength). The Aerogel was affected from the

chromatic point of view, however, its structure remained rather similar to the unheated specimen.
In both cases, the yellowish-brownish colour can be attributed to the partial combustion of the polymeric parts, as seen in the relative test (smoke release), as well as melting and decomposition (in the case of EPS).

Figure 7. Zoomed photos. From left to right: initial EPS.m, post-heating EPS.m, initial Aero.m, post-heating Aero.

iii) Scanning electron microscope (SEM)

According to XRD, Aero.m at initial conditions (pre-heating) contain calcite (hydraulic lime or cement), gehlenite (hydraulic compound of cement), and gypsum. In image a), one can see acicular compounds at the interfaces between a siliceous aggregates and the cementitious matrix, which must correspond to the hydraulic compounds mentioned above. The aerogel has a compact microstructure, with some micro-cracks. Spherical particles may correspond to other compounds in the formulation (e.g. perlite, undetected in the XRD, being amorphous). Regarding TGA analysis data (section 3.2), the mass loss was considerably lower than EPS.m, which shows its thermal stability in the considered temperature range.
After heating (300° C, Figure 8 (left)), the images show an increase in microporosity, possibly dependent on the dehydration of the cementitious products of the matrix, however, the mictostructure is rather similar to the initial unheated sample. Dehydration is also confirmed by XRD, by the disappearance of gehlenite and gypsum.

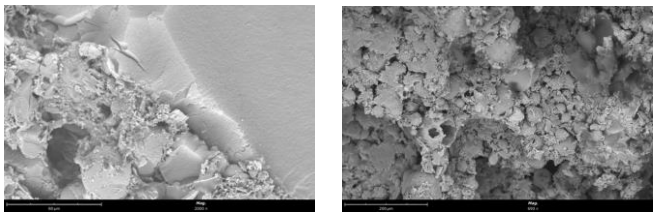

Figure 8. SEM images of Aero.m; initial conditions (left), post heating (right)

Regarding EPS.m, initially (pre-heating) - Figure 9 (left), the matrix shows a high porosity, but generally a compact morphology (expanded polystyrene with some cohesion with the calcite-based binder). XRD confirmed a constitution mostly based on calcite (originally natural hydraulic lime). After heating, the formation of metastable phases of $CaCO_3$, e.g. aragonite and vaterite, was confirmed by XRD. As analysed in TGA, the expanded polystyrene undergoes an important thermochemical degradation, accompanied by shrinkage (polystyrene, when expanded, can increase by 50 times its volume; after heating, it exponentially shrinks again, if compared to its expanded state). The SEM images post-heating (Figure 9 (right)) confirmed the macroscopic and tomographic observations, which indicate that there are still residues resulting from the incineration of polystyrene in the matrix (total decomposition around 450°C). On the other hand, the microstructure is maintained, with apparently global preservation of the porous matrix.

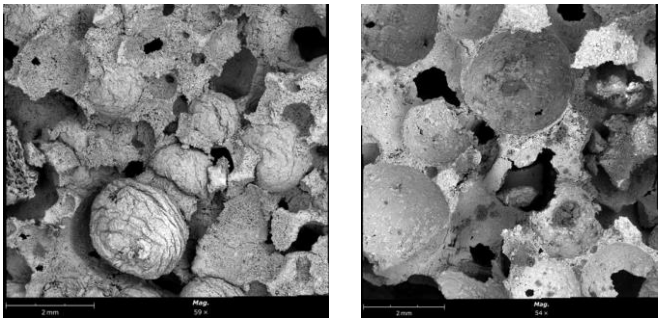

Figure 9. SEM images of EPS.m; initial conditions (left), post heating (right)

3.4 Fire reaction tests

During the ignitability test performed to the thermal mortar with aerogel, neither ignition of the sample nor residues on the filter paper placed on the base of the specimens were observed. There was also no release of flaming droplets or particles. This procedure only allowed to conclude that the material is, at least, classified as E.
When it comes to the Gross Calorific Potential test conducted on samples of the mortar with aerogel, the PCS (gross calorific potential) value obtained was 6.19 ± 0.25 MJ/Kg, which is significantly above the maximum permitted value to be able to classify a material as A2 (3 MJ/Kg [29]) . However, the bomb calorimeter test, which is not standardized but allows the measurement of the same variable, provided significantly different results. Indeed, the value obtained was 4.3 MJ/Kg.
Although both results provide values above the standard's threshold to classify the product as A2, there are relevant conclusions that we can draw. Since the sample used for both procedures only have a few milligrams, they may not be representative of a future practical use of the mortar. Furthermore, not being a commercial product yet, it is not optimized, nor there is a manufacturing production method that ensures a proper control of the quantities and proportions of reagents which means that some lack of homogenization may have occurred during specimens' production.
The cone calorimeter results indicate how fast the specimens ignite. The performed heat fluxes were 13.64, 15.82, 17.55 and 22.36 KW/m^2. The EPS.m only ignited for the two higher heat fluxes, which means that the critical heat flux, i.e. the minimum heat flux for material to ignite, should be within the range 17.55-15.82 KW/m^2. Lower heat releases rates should have been studied for Aero.m since it has ignited for the lowest heat flux analyzed. However, due to time constrains regarding the use the equipment in DTU's laboratory, it was not possible to repeat these tests using different heat fluxes.
The results show that Aero.m has the fastest delay time which means it ignites earlier than EPS.m. Such result was not expected because: i) in the standardized ignitability test (performed at ITECONS) the specimen, Aero.m, did not ignite when exposed directly to a small flame; ii) during the previous experiments EPS.m has proven to be more susceptible to high temperatures presenting a higher mass loss (TGA), higher disaggregation level on residual compressive strength test; iii) due to the higher polymeric content of EPS.m when comparing to Aero.m.
Another unexpected event was the non-ignition of Aero.m for a heat release of 22.36 KW/m^2. Since it has ignited for lower heat releases, for 17.55 KW/m^2 it only took 8 s for the ignition to start, it was estimated the ignition would start in less than 8 s with 22.36 KW/m^2. However, it did not happen. These,

apparently, incoherent results may be stem from the fact that Aero.m is a non-commercial mortar with a non-controlled production, therefore some lack of homogenization may have occurred causing the polymeric content, which is what contributes as a combustible material, to get concentrated on top of the specimen, triggering the ignition to happen for heat flux of 17.55 KW/m^2.

3.5 Fire exposure tests

Figure 10 shows that the lime-based mortar and the Aero.m presented an overall more gradual temperature increase than the EPS mortar. Regarding the thermal mortars (EPS.m and Aero.m), two distinct behaviors are observed: (i) a first one up to about 100° C, in which the temperature increases at a lower rate (when compared to the one afterwards); at this temperature a plateau is observed that corresponds to the evaporation of water, a plateau that is longer (in time) the more it advances in the mortar thickness (in relation to the exposed surface); for example, at 2 cm from the heat source this plateau lasts about 17 min (1000 s) and at 4 cm about 30 min (1800 s); (ii) and a second characterized by a higher temperature increase rate. In the case of the EPS mortar, an abrupt temperature increase from 100°C to about 400°C is observed at mid-thickness (i.e. at 2 cm), lasting 8 min. This finding may be related to the decomposition of the polymeric compounds, namely the EPS particles that, during this process release energy and contribute to this abrupt increase. In fact, the results within this temperature range agree with the peaks observed in the TGA results (cf. section 3.2), which may reinforce the veracity of this cause-effect relationship.

A similar behaviour is observed in Aero.m, which, however, in a more detailed and amplified evaluation shows some differences to EPS.m. Analysing the curves at mid-thickness of the specimens (Figure 10b), it is clear that Aero.m presents a better insulating capacity than EPS.m; this conclusion is evident, for example, by the longer time required to reach 200°C (1100s for EPS.m vs. 1300s for Aero.m). Furthermore, this figure shows that from 120°C the lime mortar presents the lowest temperature increase rate; this result should be related to its (mostly) inorganic composition, and therefore less susceptible to changes caused by exposure to high temperatures.

In the initial test conditions, at room temperature, the Lime.m thermal conductivity values are the highest, suggesting that higher temperatures were reached in the specimen of this mortar. However, according to the graph in Figure 10b) it can be observed that both at mid-thickness of the specimen (elevation 2), and on the surface in contact with air (elevation 4), the lime mortar reaches the lowest temperatures. This result indicates that the thermophysical properties (thermal conductivity, density and specific heat) at elevated temperatures of the lime mortar result in a more stable material. This reversal of hierarchy at the level of thermophysical properties is noticeable from 120°C (Figure 10b)) and is justified by the fact that the EPS particles and polymeric components of the aerogel mortar decompose with temperature, compromising the insulating capacity of these mortars.

Finally, it is worth noting that the thermal distribution described in this section were also used as input data in a numerical procedure (described in chapter 5) to calibrate the thermal properties of the mortars at elevated temperatures using an inverse analysis.

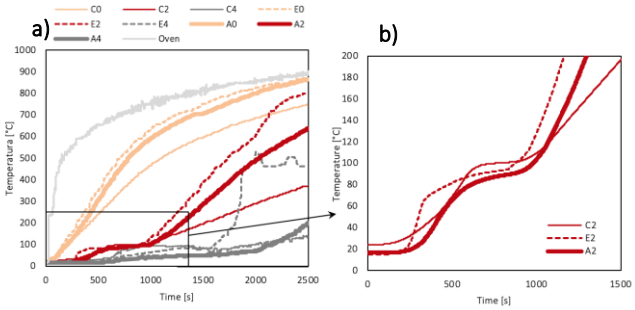

Figure 10. Fire exposure curves a) of the analysed mortars, b) focusing on the initial part of the test and the specimens' half thickness (dimension 2 cm). The colours refer to the thermocouple height (e.g. C0 = thermocouple in contact with the steel plate; C1, C2, C3, C4 = thermocouples installed at 1 ,2, 3, 4 cm from the plate); C – Lime.m, E – EPS.m, A – Aero.m

4 Numerical analyses

Following the fire exposure tests described in section 2.2.5, the present chapter describes the analytical-numerical study that was developed in order to determine the thermophysical properties (thermal conductivity and specific heat) as a function of temperature of the mortars under study, through an inverse analysis.

For that end, it was necessary to use (i) a 1D thermal finite element model [30] and (ii) an optimisation routine. The former was used to obtain numerical simulation of the tests performed whereas the second was used to perform comparisons between the numerical and experimental results and iteratively approximate both responses by modifying the (unknown) thermophysical properties of the mortars at different elevated temperatures (these were initially assumed to be constant with temperature, and then considered as temperature-dependent).

Figure 11 presents the obtained thermophysical properties (thermal conductivity and specific heat) in function of temperature of the mortars at the end of the numerical procedure.

For all 3 mortars, the thermal conductivity progression shows similar peaks. It starts with an abrupt increase in conductivity up to 100°C (possibly related to the water evaporation process), followed by a decrease between 200°C and 300°C. Finally, there is a moderate increase until 400°C followed by another decrease where thermal mortars reach the initial values and the Lime.m shows a value slightly higher than the initial one.

Aero.m seems to be the one that undergoes the least changes, i.e., the one that is less affected by the temperature increase. On the other hand, Lime.m is the one that presents the largest peak, at 100°C, in which conductivity almost quadruples in value.

As far as the specific heat is concerned, there is initially a steep increase, where the specific heat peaks between 100 and 200°C; the values at very high temperature are approximately the same to those at ambient temperature conditions. These peaks can be associated to the thermal decompositions; there they generally endothermic (heat consuming) processes as physical theory suggests [31]; this means that when the material is decomposing a lot of energy needs to be provided (*Cp* peaks) in order to decompose the material and to increase

its temperature. In this sense it is possible to justify the fact that EPS.m has the highest peak since it has a large percentage of polymeric (organic) components. Although aerogel is an inorganic material, the Aero.m mortar also has polymeric content, thus the peaks observed in the *Cp* (although with lower magnitude than those of the EPS.m).

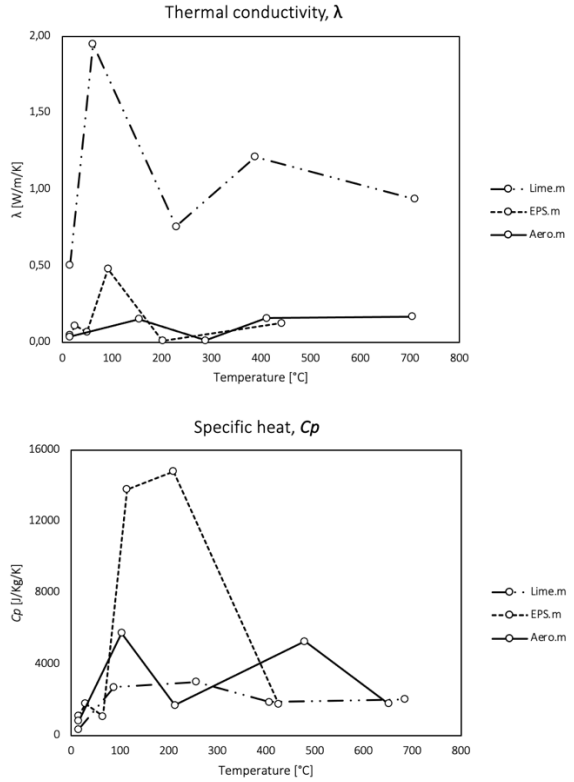

Figure 11. Thermal conductivity and specific heat in function of temperature

5 Conclusions and future developments

The results of the material characterization tests, (i), showed that both the conventional (with EPS) and the innovative thermal mortar (with aerogel) are thermally unstable, due to the susceptibility of their constituents when subjected to high temperatures, especially due to their polymeric adjuvants/components. Regarding Aero.m, despite the referred instability, its residual mass at 800°C was considerably higher than that of EPS.m, showing that its constituents (in particular the aerogel) are less degraded by exposure to high temperatures than the EPS particles. The results obtained for Lime.m showed that, as expected, its constituents are less affected by temperature, however, this mortar does not comply with requirements (considering EN 998-1) to be classified as a thermal mortar.

Through the microstructural analyses, (ii), it was possible to accomplish that, on both thermal mortars, the binder matrix presented few alterations due to the exposure to high temperatures. In fact, whereas the lightweight aggregates (EPS granules) in EPS.m were completely decomposed, the aerogel particles in Aero.m only presented some micro-cracks. It was concluded that the thermal susceptibility of Aero.m was mainly caused by its polymeric additives. It is worth mentioning that Aero.m is a non-commercial product and its formulation (i.e. constituents) is not optimized considering its fire behaviour, nonetheless the results pointed out that there is a considerable potential on aerogel-based thermal mortars as an alternative to EPS-based solutions.

The fire reaction tests (iii) carried out can be divided in two categories: (a) the ones that were developed according to the standardized procedures, and (b) the complementary ones. Regarding (a), it was possible to concluded that Aero.m will be classified below class A2 and above Euroclass E. Although it has not been possible to performed all standardized tests required to define a specific fire reaction class (as they would involve a significant amount of material and costs), during the ignitability test there was an important observation - the sample did not ignite when exposed to the small flame action, which seems promissory on avoiding fire spread on facades. Regarding the cone calorimeter experiments, (b), the results were not in line with the ignitability ones since samples of Aero.m ignite earlier than EPS.m. Unfortunately, as these tests were carried out during the stay in DTU (Denmark) and due to time constrains, it was not possible to repeat these tests; therefore, further research is needed in the cone calorimeter experiments with new samples.

The results of the fire exposure tests confirmed that EPS.m presents a worse insulating capacity during fire exposure than Aero.m by the shorter time required to reach 200°C in half-thickness of the samples (1100s for EPS.m vs. 1300s for Aero.m); this result may be a consequence of the decomposition of its polymeric compounds and, in particular, of the EPS particles. During the experimental procedures, EPS.m sample released a higher amount of smoke and stronger smell than Aero.m. A more accurate analyses on these parameters was not carried out due to lack of time, material and proper instrumentation for the analysis of the smoke released.

The study developed within this dissertation showed the potential danger of using EPS-based mortar in facades, especially because of their low fire performance, highlighting the need to develop alternative thermal mortars; in this context, it was showed that aerogel-based renders have the potential to be an alternative to the EPS-based ones, presenting an improved fire performance.

The results obtained suggest analyzing the gaps of performance in Aero.m by comparing it with commercial mortars and testing new formulations, followed by the new fire behavior tests on this new formulation and then the evaluation of the entire system.

The development of optimized formulations of aerogel-based thermal mortars, accompanied by specific tests to determine their reaction to fire class, will contribute to improve the safety of buildings with these systems and to expand the field of application of these innovative mortars.

6 References

[1] United Nations, Global Alliance for Buildings and Construction 2020 Global Status Report for Buildings and Construction Towards a zero-emissions, efficient and resilient buildings and construction sector, 2020. http://www.un.org/Depts/.

[2] N. White, M. Delichatsios, M. Ahrens, A. Kimball, Fire hazards of exterior wall assemblies containing combustible components, MATEC Web Conf. 9 (2013). https://doi.org/10.1051/matecconf/20130902005.

[3] M. Bonner, G. Rein, Flammability and multi-objective performance of building façades: Towards optimum design, Int. J. High-Rise Build. 7 (2018) 363–374.

https://doi.org/10.21022/IJHRB.2018.7.4.363.
[4] N. Hopkins, Huge concentrations' of toxins found in Grenfell soil, Guard. (2018). https://www.theguardian.com/uk-news/2018/oct/12/toxins-found-ingrenfell- tower-soil-study-finds (accessed 8 September 2021).
[5] A.A. Stec, K. Dickens, J.L.J. Barnes, C. Bedford, Environmental contamination following the Grenfell Tower fire, Chemosphere. 226 (2019). https://doi.org/10.1016/j.chemosphere.2019.03.153.
[6] J. Alemán, A. V. Chadwick, J. He, M. Hess, K. Horie, R.G. Jones, P. Kratochvíl, I. Meisel, I. Mita, G. Moad, S. Penczek, R.F.T. Stepto, Definitions of terms relating to the structure and processing of sols, gels, networks, and inorganic-organic hybrid materials (IUPAC recommendations 2007), Pure Appl. Chem. 79 (2007) 1801–1829. https://doi.org/10.1351/pac200779101801.
[7] M. Rubin, C.M. Lampert, Transparent silica aerogels for window insulation, Sol. Energy Mater. 7 (1983) 393–400. https://doi.org/10.1016/0165-1633(83)90012-6.
[8] S.Q. Zeng, A.J. Hunt, W. Cao, R. Greif, Pore Size Distribution and Apparent Gas Thermal Conductivity of Silica Aerogel, J. Heat Transfer. 116 (1994) 756–759. https://doi.org/10.1115/1.2910933.
[9] G.M. Pajonk, Transparent silica aerogels, J. Non. Cryst. Solids. 225 (1998) 307–314. https://doi.org/10.1016/S0022-3093(98)00131-8.
[10] A. Soleimani Dorcheh, M.H. Abbasi, Silica aerogel; synthesis, properties and characterization, J. Mater. Process. Technol. 199 (2008) 10–26. https://doi.org/10.1016/J.JMATPROTEC.2007.10.060.
[11] E. Strobach, B. Bhatia, S. Yang, L. Zhao, E.N. Wang, High temperature stability of transparent silica aerogels for solar thermal applications, APL Mater. 7 (2019) 081104. https://doi.org/10.1063/1.5109433.
[12] U. Berardi, Aerogel-enhanced systems for building energy retrofits: Insights from a case study, Energy Build. 159 (2018) 370–381. https://doi.org/10.1016/J.ENBUILD.2017.10.092.
[13] T. Stahl, S. Brunner, M. Zimmermann, K. Ghazi Wakili, Thermo-hygric properties of a newly developed aerogel based insulation rendering for both exterior and interior applications, Energy Build. 44 (2012) 114–117. https://doi.org/10.1016/j.enbuild.2011.09.041.
[14] EMPA, Technical data sheet: Fixit 222, (2017). www.fixit.ch (accessed 26 March 2022).
[15] M. Ibrahim, E. Wurtz, P.H. Biwole, P. Achard, H. Sallee, Hygrothermal performance of exterior walls covered with aerogel-based insulating rendering, Energy Build. 84 (2014) 241–251. https://doi.org/10.1016/J.ENBUILD.2014.07.039.
[16] K. Ghazi Wakili, T. Stahl, E. Heiduk, M. Schuss, R. Vonbank, U. Pont, C. Sustr, D. Wolosiuk, A. Mahdavi, High performance aerogel containing plaster for historic buildings with structured façades, Energy Procedia. 78 (2015) 949–954. https://doi.org/10.1016/J.EGYPRO.2015.11.027.
[17] M. Pedroso, I. Flores-Colen, J.D. Silvestre, M.G. Gomes, L. Silva, L. Ilharco, Physical, mechanical, and microstructural characterisation of an innovative thermal insulating render incorporating silica aerogel, Energy Build. 211 (2020) 109793. https://doi.org/10.1016/j.enbuild.2020.109793.
[18] Enersens, Product data sheet: Aerogel kwark, (2015). available: http://enersens.fr/en/home/.
[19] M. Pedroso, Eco-efficient and multifunctional thermal renders based on silica aerogel and fibres - Phd Thesis, Instituto Superior Técnico, 2021.
[20] Saint-Gobain Weber, Technical data sheet: Webercal classic (in Portuguese), (2020). www.pt.weber.
[21] Saint-Gobain Weber, Technical data sheet: WeberTherm Aislone (in Portuguese), (2018). www.weber.com.pt.
[22] International Organization for Standardization, ISO 834-1: Fire-Resistance Tests - Elements of Building Construction - Part 1: General Requirements, (1999).
[23] CEN, EN 1015-11: Methods of test for mortar for masonary - Part 11: Determination of ŕexural and compressive strength of hardened mortar, (1999).
[24] Applied Precision Ltd., Isomet 2114 Thermal properties analyser user's guide, Version 1.46, (2011). www.Manualslib.com.
[25] American Society for Testing Materials, ASTM E119-11: Standard Test Methods for Fire Tests of Building Construction and Materials, (2010).
[26] CEN, EN 1015-10: 1999 - Methods of test for mortar for masonry - Part 10: Determination of dry bulk density of hardened mortar, (1999).
[27] Z. Wu, K.H. Khayat, C. Shi, B.F. Tutikian, Q. Chen, Mechanisms underlying the strength enhancement of UHPC modified with nano-SiO2 and nano-CaCO3, Cem. Concr. Compos. 119 (2021) 103992. https://doi.org/10.1016/j.cemconcomp.2021.103992.
[28] E. Tajuelo Rodriguez, K. Garbev, D. Merz, L. Black, I.G. Richardson, Thermal stability of C-S-H phases and applicability of Richardson and Groves' and Richardson C-(A)-S-H(I) models to synthetic C-S-H, Cem. Concr. Res. 93 (2017) 45–56. https://doi.org/10.1016/j.cemconres.2016.12.005.
[29] CEN, EN 13501-1: Fire classification of construction products and building elementes - Part 1: Classification using data from reaction to fire teste, (2009).
[30] C. Sánchez, Numerical modelling of the thermomechanical behaviour of GFRP pultruded profiles subjected to fire, Universidade de Lisboa - Instituto Superior Técnico, 2017.
[31] D. V. Schroeder, J.K. Pribram, An Introduction to Thermal Physics, Am. J. Phys. 67 (1999) 1284–1285. https://doi.org/10.1119/1.19116.